eNeuro

Research Article: Methods/New Tools | Novel Tools and Methods

Characterization of a Knockin Mouse Line Expressing a Fusion Protein of Kappa Opioid Receptor Conjugated with tdTomato: 3-Dimensional Brain Imaging Via CLARITY

https://doi.org/10.1523/ENEURO.0028-20.2020

Cite as: eNeuro 2020; 10.1523/ENEURO.0028-20.2020

Received: 28 January 2020
Revised: 2 June 2020
Accepted: 5 June 2020

Characterization of a Knockin Mouse Line Expressing a Fusion Protein of Kappa Opioid Receptor Conjugated with tdTomato: 3-Dimensional Brain Imaging Via CLARITY

Abbreviated title: 3-D imaging and cellular localization of KOR in brain

Chongguang Chen, Alex H. Willhouse, Peng Huang, Nora Ko, Yujun Wang, Bin Xu[1], Lan Hsuan Melody Huang, Brigitte Kieffer[2], Mary F. Barbe[3], and Lee-Yuan Liu-Chen

Center for Substance Abuse Research and Department of Pharmacology, [1]Cardiovascular Research Center, [3] Department of Anatomy and Cell Biology, Lewis Katz School of Medicine, Temple University, Philadelphia, PA 19140
[2]Douglas Hospital, McGill University, Verdun, Quebec H4H 1R3, Canada

Corresponding author email address: Lee-Yuan Liu-Chen, Ph.D., Center for Substance Abuse Research, Temple University Lewis Katz School of Medicine, 3500 North Broad Street, MERB 851, Philadelphia, PA 19140, USA. lliuche@temple.edu

Number of pages
Number of figures (8), table (1), and supplementary figures (4)
Number of words for abstract (246), introduction (628), and discussion (1563)

Conflict of interest statement: The authors declare no competing financial interests

Acknowledgments: This work was supported by NIH grants R01 DA041359, R21 DA045274, R03 DA036802 and P30 DA013429. We thank Dr. George Smith of Temple University Lewis Katz School of Medicine for scAAV2-GFP tracer.

Abstract

Activation of kappa opioid receptor (KOR) produces analgesia, antipruritic effect, sedation and dysphoria. To characterize neuroanatomy of KOR at high resolutions and circumvent issues of specificity of KOR antibodies, we generated a knock-in mouse line expressing KOR fused at the C-terminus with the fluorescent protein tdTomato (KtdT). The selective KOR agonist U50,488H caused anti-scratch effect and hypolocomotion, indicating intact KOR neuronal circuitries. Clearing of brains with CLARITY revealed 3-dimensional (3-D) images of distribution of KOR, and any G protein-coupled receptors, for the first time. 3-D brain images of KtdT and immunohistochemistry (IHC) on brain sections with antibodies against tdTomato show similar distribution to that of autoradiography of [^{3}H]U69,593 binding to KOR in wildtype mice. KtdT was observed in regions involved in reward and aversion, pain modulation and neuroendocrine regulation. KOR is present in several areas with unknown roles, including the claustrum, dorsal endopiriform nucleus, paraventricular nucleus of the thalamus, lateral habenula and substantia nigra pars reticulata (SNr), which are discussed. Prominent KtdT-containing fibers were observed to project from caudate putamen (CP) and nucleus accumbens (ACB) to substantia innominata (SI) and SNr. Double IHC revealed co-localization of KtdT with tyrosine hydroxylase (TH) in brain regions, including CP, ACB and ventral tegmental area (VTA). KOR was visualized at the cellular level, such as co-localization with TH and agonist-induced KOR translocation into intracellular space in some VTA neurons. These mice thus represent a powerful and heretofore unparalleled tool for neuroanatomy of KOR at both the 3-D and cellular levels.

Significance Statement

A combination of tagging KOR with tdTomato and tissue clearing with CLARITY enables 3-D mouse brain imaging of KOR, or any G protein-coupled receptors, for the first time. This approach reveals prominent KOR-expressing fiber bundles from caudate putamen and nucleus accumbens to substantia nigra pars reticulata and allows visualization of the KOR at the cellular level, including co-localization with TH and agonist-induced KOR

translocation in some neurons. Regions expressing moderate to high KOR, but with no known functions, are highlighted and discussed, including claustrum, dorsal endopiriform nucleus, paraventricular nucleus of the thalamus and lateral habenula. The mouse line will be a valuable tool for investigation of KOR neurobiology. This approach paves ways for future similar studies.

Introduction

Activation of the KOR produces many effects, including analgesia, antipruritic effect, dysphoria/aversion, sedation, water diuresis and hypothermia (von Voigtlander et al., 1983; Simonin et al., 1998; Cowan et al., 2015). The selective KOR agonist nalfurafine is used in Japan for treatment of pruritus in kidney dialysis or chronic liver disease patients (Nakao and Mochizuki, 2009; Kamimura et al., 2017). In addition, KOR agonists may be useful as analgesics and water diuretics. KOR antagonists produce anxiolytic- and antidepressant-like effects in animal models (Carlezon et al., 2009; Bruchas et al., 2010; Carr et al., 2010) and may be useful in alleviating drug craving in addicts (Shippenberg et al., 2007; Bruchas et al., 2010; Wee and Koob, 2010).

Localization of KOR protein in brains has been investigated with receptor autoradiography and IHC. Autoradiography of binding of the selective KOR radioligand [^{3}H]U69,593 or [^{3}H]CI-977 has provided an excellent map of receptor distribution in the brain (Mansour et al., 1988; Slowe et al., 1999). Because of high KOR selectivity of the radioligand, receptor autoradiography has high specificity; however, the resolution is low, which does not allow visualization at the cellular level. IHC of KOR has been performed, but different KOR antibodies have yielded different results [for example, (Arvidsson et al., 1995; Drake et al., 1996; Mansour et al., 1996; Appleyard et al., 1997)]. Two KOR antibodies (KT2 and KOR1) (Arvidsson et al., 1995; Drake et al., 1996) are more widely used and thus discussed here. KT2 and KOR1 were raised against the rat KOR 371-380 and 366-380 peptides, respectively. As discussed by (Drake et al., 1996), the two antibodies revealed similarities and significant differences in KOR distribution and staining intensity. Both antibodies labeled several brain regions that have high [^{3}H]U69,593 binding. However, neither labeled claustrum (CLA), which

92 has the highest [^{3}H]U69,593 binding in the brain (Unterwald et al., 1991; Wang et al.,
93 2011). On the other hand, the striatum contained high KOR1, but low KT2
94 immunoreactivity. At the ultrastructural level, KOR1-IR was localized to cell bodies and
95 dendrites, whereas KT2-IR was found mostly in axons. The specificity of KOR
96 antibodies from commercial sources were not adequately validated, like most
97 commercially available antibodies against other G protein-coupled receptors [for
98 example, (Michel et al., 2009)].
99 Conventional neuroanatomy methods for receptor localization, such as receptor
100 autoradiography and IHC, are performed on brain sections, thus producing 2-
101 dimensional images. Advancements in tissue clearing with CLARITY render tissue
102 optically transparent, yet retain tissue integrity, thus allowing 3-D imaging (Chung and
103 Deisseroth, 2013; Chung et al., 2013; Tomer et al., 2014). CLARITY involves perfusion
104 of animals with fixatives and acrylamide-based hydrogel, cross-linking of hydrogel with
105 proteins and nucleic acids and removal of lipid by detergents. CLARITY-cleared tissues
106 can be imaged with or without further processing.
107 To generate 3-D KOR distribution in brain and to circumvent the low resolution of
108 receptor autoradiography and the problems associated with KOR antibodies, we
109 generated a knockin mouse line expressing the KOR fused at the C-terminus with
110 tdTomato (tdT) (KtdT). Similar approaches have been used to generate knockin mouse
111 lines expressing the delta opioid receptor or nociceptin / orphanin FQ receptor fused
112 with enhanced green fluorescent protein (Scherrer et al., 2006; Ozawa et al., 2015) or
113 the mu opioid receptor conjugated with mCherry (Erbs et al., 2015). We previously
114 generated a mouse KtdT construct and found that when expressed in Neuro2A mouse
115 neuroblastoma cells, mKtdT exhibited similar binding, signaling and translocation as
116 FLAG-mKOR (Huang et al., 2013).
117 Here we report generation and characterization of the KtdT mice, including
118 behavioral responses, receptor protein and mRNA expression levels, KtdT distribution,
119 possible co-localization with TH and agonist-induced translocation of KOR. KtdT
120 distribution was examined with 3-D images of the KOR following clearing of brains with
121 CLARITY, but without IHC, and IHC with antibodies against tdT on brain sections.
122

Methods and Materials

Antibodies and viral vector

Rabbit anti-red fluorescent protein (RFP) antibody was purchased from Rockland (catalog no. 600-401-379, Limerick, PA). Chicken antibodies against tyrosine hydroxylase (anti-TH) was from Abcam (ab76442, Cambridge, MA). Goat anti-rabbit IgG conjugated with Alexa 594 (A11012) and goat anti-chicken IgG conjugated with Alexa 488 (A11039) were from ThermoFisher / Life Technologies (Waltham, MA). scAAV2-GFP tracer (Liu et al., 2014) (titer>10^{13} GC/ml) was a generous gift from Dr. George Smith of Temple University Lewis Katz School of Medicine.

Materials

U50,488H and naloxone were obtained from the National Institute on Drug Abuse Drug Supply Program (Rockville, MD). [^{3}H]U69,593 (60 Ci/mmol) was purchased from PerkinElmer Life Sciences (Boston, MA). The following reagents were obtained from indicated companies: VectaShield mounting media, Vector Labs (Burlingame, CA); RNAeasy Mini kit, Qiagen (Waltham, MA); Superscript II, ThermoFisher / Invitrogen (Waltham, MA); iQ SYBR green supermix, Bio-Rad (Hercules, CA); Urea (8.18710), EMD Millipore (Billerica, MA) The following materials were purchase from Sigma-Aldrich (St. Louis, MO): paraformaldehyde (PFA), compound 48/80, Kolliphor EL, phenylmethylsulfonyl fluoride, Quadrol (#122262), Triton X-100 (T8787), Histodenz (D2158). Other commonly used chemicals were obtained from Sigma-Aldrich or ThermoFisher Scientific.

Generation of KtdT knockin mice

A targeting vector was constructed in which the KOR (K) gene (Oprk1) was modified so that a floxed neomycin resistant gene was inserted in the intron upstream of the exon 4 and Gly-Ser-Ile-Ala-Thr-tdTomato encoding cDNA was inserted immediately 5' to the stop codon in the exon 4 (Fig. 1A). The targeting strategy was similar to those of (Scherrer et al., 2006) and (Ozawa et al., 2015). This construct was then transfected into embryonic stem (ES) cells. A positive ES clone with proper homologous recombination was electroporated with a Cre-expressing plasmid to excise the

neomycin gene and subsequently microinjected into C57BL/6N blastocysts. The resulting animals were cross-bred with C57BL/6N mice to obtain F1 heterozygous progenies. Heterozygous mice were intercrossed to generate homologous KtdT mice (KtdT/KtdT). KtdT/KtdT mice were fertile and developed normally. Male and female homozygous (KtdT/KtdT), heterozygous (KtdT/K) or their wild-type (K/K) littermates weighing 20–23 g (8- 12 weeks old) were used. Breeding was also carried out among KtdT/KtdT mice and among K/K mice. Animals were group-housed under standard laboratory conditions and kept on a 12 h day/night cycle (lights on at 7:00 A.M.). Mice were maintained in accordance with the National Institutes of Health Guide for the Care and Use of Laboratory Animals. All methods used were preapproved by the Institutional Animal Care and Use Committee at the Temple University.

Mouse genotyping was carried out by PCR with total DNA isolated from mouse ears. To detect the excision of the selection marker of knockin allele, the primer pair Ef/Er was used [5'-GATGCTGTTAATCACAGTGAGCTG -3' (forward) / 5'-CCCACAACCATAGCTCTGACAAGAG-3' (reverse)] as diagramed in Fig. 1B.

Brain membrane preparation and binding of [^{3}H]U69,593 to the KOR in membranes

Frozen mouse whole brains were homogenized in ~8-volumes of 25 mM Tris-HCl buffer, pH 7.4 containing 1 mM EDTA and 0.1 mM PMSF on ice and then centrifuged at ~100,000 g for 30 min. Pellets were twice rinsed with 25 mM Tris-HCl buffer and re-suspended in 0.32 M sucrose in 50 mM Tris-HCl, pH 7.0. Suspended membranes were passed through a 26.5 G needle 5 times and then frozen at −80°C. KOR binding experiments were performed with [^{3}H]U69,593 (~4.5 nM) on brain membranes (1.8 mg membrane proteins). Non-specific binding was determined in the presence of naloxone (10 μM).

Determination of KOR mRNA levels by quantitative reverse transcription-polymerase chain reaction (qRT-PCR)

Total RNA was isolated from mouse brains using RNAeasy Mini kit (Qiagen). Total RNA from brain was reverse-transcribed with Superscript II reverse transcriptase

(Invitrogen) and random primers. cDNA was used in PCR experiments performed with CFX Real-Time PCR system (Bio-Rad Laboratories) by using iQ SYBR green supermix (Bio-Rad). Primers for PCR were 5'-ATCACCGCTGTCTACTCTGTGG-3' (forward) and 5'-GTGGTAGTAACCAAAGCATCTGC-3' (reverse) (http://www.origene.com/qPCR/primer_pair/MP210416.aspx), encompassing exons 2 and 3 of oprk1 gene (www.ensembl.org) and producing a 149-bp fragment from KOR cDNA. GAPDH was used as a housekeeping gene and relative KOR mRNA levels were calculated.

Determination of U50,488H-induced anti-scratching activities in mice

Experiments were performed according to our published procedures (Liu et al., 2019). Briefly, after habituation to observation boxes (1 mouse/box) for 1 hour, mice were administered subcutaneously (s.c.) vehicle or U50,488H at an indicated dose and 20 minutes later, injected with 0.1 ml of compound 48/80 (0.5 mg/ml, 50 μg, s.c.) into the nape. The number of bouts of hind leg scratching of the neck was counted for 30 minutes. The relative percentage of scratching was calculated as follows:

$$\frac{mean\ number\ of\ scratches\ by\ treatment\ group}{mean\ number\ of\ scratches\ by\ control\ group}\ x\ 100\%$$

Typically, saline-treated mice scratched 260 ± 30 (mean ± S.E.M.) times. A_{50} value of U50,488H was determined by plotting dose against % scratch and using linear regression to obtain a best-fit line (Prism 6.0, GraphPad Software, La Jolla, CA).

Measurement of locomotor activities

Locomotor activities were measured as described previously (Xu et al., 2013; Liu et al., 2019) using a Locomotor Activity System (Omnitech Electronics Inc., Columbus, OH) and eight individual activity monitors. Briefly, mice were treated with saline or U50,488H (s.c.) at indicated doses and placed into locomotor chambers immediately. Locomotor activities were continuously monitored for 60 minutes and data were recorded continuously for 5-min intervals.

IHC

Tissue fixation by perfusion of mice with 4% PFA: Adult male and female KtdT/KtdT and K/K C57BL/6N mice of 2-3 months old were deeply anesthetized with sodium pentobarbital (7.8 mg /30 g) and perfused transcardially with 10-20 ml 0.1 M phosphate buffered saline (1x PBS) (pH7.4) followed by ~100 ml 4% PFA solution in in 0.1 M phosphate buffer (1x PB) (pH7.4). Brains were dissected, post-fixed in 4% PFA in 1x PB overnight and then placed in 30% sucrose for up to 72 hours for cryoprotection.

IHC: Brains were frozen in O.C.T. and sectioned with a cryostat (Leica CM3050S) at a thickness of 30 µm at -18ºC and placed in 10 mM PBS [8.2 mM Na_2HPO_4, 1.8 mM KH_2PO_4, NaCl 134 mM, KCl 2.7 mM, pH7.5] plus 0.05 NaN3% for short-term storage at 4ºC. Sections were rinsed with 10 mM PBS 5 x 5 minutes, blocked for one hour at room temperature with the blocking buffer [5% normal goat serum, 0.1 M glycine and 0.3% Triton X-100 in 10 mM PBS]. Sections were incubated with rabbit anti-RFP at 1/1000 in the staining buffer [3% BSA, 0.3% Triton X-100 in 10 mM PBS] at 4ºC overnight and washed 5X5 min with 10 mM PBS. Sections were then incubated with AlexaFluor594-conjugated goat anti-rabbit IgG (1/1000) overnight at 4ºC and washed 5X5 min with 10 mM PBS. Sections were subsequently mounted on fluorescence-free glass slides with Vectashield containing DAPI and placed at 4ºC for storage for up to 2 months. Sections were examined under a fluorescence microscope (Nikon, ECLIPSE TE300) and some were further examined under a confocal microscope (Nikon A1R).

Double IHC: sections were incubated with rabbit anti-RFP at 1/1000 and chicken anti-TH at 1/1000 overnight. Following washes, sections were incubated with AlexaFluor594-conjugated goat anti-rabbit IgG (1/1000) and AlexaFluor488-conjugated goat anti-chicken IgG (1/1000). After washing, sections were mounted and examined as described above.

Autoradiography of [^{3}H]U69,593 binding to KOR in coronal brain sections

The experiments were performed per our published procedures (Wang et al., 2011; Van't Veer et al., 2013). Briefly, wildtype C56BL/6 mice were killed by decapitation and brains removed and immediately frozen in isopentane on dry ice. Frozen brains were cut at 20 µm to obtain coronal sections at -18ºC, which were thaw-mounted onto gelatin-subbed slides and dried in a desiccator at 4ºC. Sections were

incubated with ~5 nM [^{3}H]U69,593 with or without 10 μM naloxone in 50 mM Tris-HCl buffer (pH7.4) at room temperature for 1 hour. Slides were then rinsed three times with 50 mM Tris-HCl buffer at 4ºC and once with deionized water and then dried with cold air. Sections were then exposed to ^{3}H-sensitive phosphor screens for about 3 weeks and images on the screens were captured with a Cyclone Storage Phosphor Scanner (Packard Bioscience, Meriden, CT).

Clearing and imaging of mouse brains with Electrophoretic Tissue Clearing (ETC) -CLARITY method

To gain tissue transparency, while maintaining the integrity of the brain structure and reducing the time needed, we adapted the ETC method described by Kim et al. (2015).

Fixation and hydrogel polymerization. Mice were anesthetized and intra-cardiacally perfused with hydrogel solution (4% PFA, 2% acrylamide, 0.25% VA-044 in 0.1M PB, pH 7.4). Brains were dissected immediately, immersed in the hydrogel solution for 3 days at 4°C with mild shaking. The tissue was then transferred to a 50-ml tube containing fresh hydrogel solution and set up in a vacuum desiccator connected to a vacuum pump and a nitrogen tank through a three-way valve. Hydrogel polymerization was initiated by applying vacuum to the desiccator for 15 min. The line was then switched to nitrogen and the tube was tightened immediately after the desiccator was filled with nitrogen gas. The polymerization was finalized after incubation of the tube for 2 h at 37°C. The fixed brains were washed and stored in PBS containing 0.1% Triton X100 and 0.02% sodium azide at 4°C for clearing.

Clearing. We constructed a 'core' device by assembling two electrode chambers and one sample chamber made of acrylic plastic blocks (Grainger). The sample chamber was separated from the electrode chambers by dialysis membrane (Spectra/Por, #132655) and sealed by silicon rubber gasket. The brain was enveloped and thermo-sealed in polyethylene mesh and attached to the minute handle shaft of a high torque clock. The brain was then inserted in and assembled with the sample chamber and driven at 60 min per rotation. We utilized common laboratory instruments mainly composed of a power supply (Bio-Rad, PowerPac HC), two refrigerated

condensation traps (Savant), and two peristaltic pumps (Cole-Parmer) for buffer cooling and circulation. The running buffer (in the electrode chambers) was composed of 25 mM boric acid adjusted to pH 9.0 with lithium hydroxide and 10 mM SDS. The clearing buffer (in the sample chamber) was identical to the running buffer except containing 200 mM SDS. Electrophoretic conditions were set at constant 120W, temperature at 15°C. With this assembly, we could fully clear a single mouse brain in 48-72 h. Some cleared brains were used for imaging directly.

Whole brains: The cleared brains were incubated with the refractive index (RI) matching medium DSMG (75g diatrizoic acid, 70g α-sorbitol, 23g N-methyl-d-glucosamine and 100g dH_2O, RI=1.46) for 3 days with mild shaking in light-tight tubes. For mounting whole brains, a sample chamber was constructed in which two cover slips were spaced and sealed by a 6.5-mm silicone isolator. The optically cleared brains were positioned horizontally in the chamber filled with DSMG media. Two image stacks were taken from ventral and dorsal directions separately using a confocal microscope (Nikon A1R). The microscopic settings were as follows: A 10X objective (NA 0.45, WD 4mm), Ch2=488 nm for autofluorescence (as the reference), Ch3=561nm for KtdT, voxel=1.66x1.66x5 μm^3, depth of v-stack or d-stack=3.5mm at Z step=5μm. Z-correction (to compensate signal reduction along Z-depth) from Z-depth 0 to 3.5 mm: laser power was set 10 to 20 for Ch3, 20 to 30 for Ch2 correspondingly; PMT HV was set 20 to 40 for Ch3, 20 to 40 for Ch2 correspondingly. The stacks were reduced to 25% of its original size for 3D reconstruction using NIS-elements and Fiji (ImageJ). The rebuilt 3D brain was presented as video clips in two views (Movie-1 and Movie-2)

1-mm sections: Cleared brains were washed with PBS (10 mM PB, pH 7.4) 3 x 2 h and then embedded in 2% agarose. Sagittal, horizontal or coronal sections were obtained using a Vibratome (Leica VT1000P) at 1-mm thickness. IHC was performed subsequently at room temperature to facilitate antibodies permeation. Sections were incubated with rabbit anti-RFP (1/200) and chicken anti-TH (1/200) for three days and washed with PBS 3 x 2h. Sections were subsequently incubated with Alexa594-conjugated goat anti-rabbit IgG (1/200) and Alexa488-conjugated goat anti-chicken IgG (1/200) in light-tight containers for 2 days followed by washing with PBS 3 x 2 h. All the

antibodies were diluted in 5% normal goat serum, 0.3% Triton X-100, 0.1 M glycine, 0.02% sodium azide in PBS (pH 7.4). The stained sections were RI-matched in Histodenz medium (80% Histodenz in 10 mM PB buffer, pH7.4 and 0.02% sodium azide, RI= 1.461) at room temperature overnight with mild shaking. Sections were mounted in the same RI media enclosed with 1-mm Silicone Isolator (JTR Press-to-Seal Silicone Isolator, 19x32 mm, Grace Bio-Labs, Inc, Bend, OR) on glass slides and cover-slipped. Imaging were performed similarly as described above. Z step was set at 5 μm and a total of about 200 steps were taken for each section. Multi-channel Images were acquired sequentially to avoid bleeding. For large images, tiles of Z stacks were acquired and stitched using NIS-elements (Nikon).

***In Situ* Hybridization (ISH)**

Tissue fixation by perfusion was performed as described under IHC. Advanced Cell Diagnostics (ACD) RNAscope Technology was used for ISH. Brains were frozen in OCT and tissue was cut at 14 μm, mounted onto Superfrost Plus slides and kept at −80°C for less than 3 months. Tissue sections was thawed at room temperature briefly, washed with 1xPBS and subsequently processed per the ACD's protocols. Tissue sections were then permeablized with solutions from the pretreatment kit and incubated with protease for 30 min and hybridization probes for another 2 h at 40°C.

Anterograde tract tracing with scAAV2-GFP tracer

Adult KtdT/KtdT mice were anesthetized with ketamine/xylazine and secured to a stereotaxic frame (Kopf, Tujunga, CA) prior to surgery. Anesthesia was maintained with 0–1% isoflurane during surgery. After incision of skin on skull, a small hole was made in the skull with a fine drill. A 33G injector (8IC315LISPCC, PlasticsOne, Roanoke, VA) was used. scAAV2-GFP tracer (0.2 μl) was delivered into the CP and ACB by an infusion pump (PHD2000, Harvard Apparatus) at a rate of 0.1 μl/min. Coordinates used were those in the atlas of Paxinos and Franklin (Paxinos and Franklin, 1997): CP (AP, 1.4 mm; ML, 1.3 mm; DV, -3.8 mm) and ACB (AP, 1.4 mm; ML, 1.3 mm; DV, -4.8 mm). Three to 4 weeks after injection, mice were perfused and fixed as described above.

U50,488-induced KOR translocation in the VTA

Adult male KtdT/KtdT mice were habituated to handling and injection by injecting (s.c.) with vehicle (water) once a day for three days. The mice were then injected via s.c. with vehicle or U50,488H in water at 5 mg/kg and 30 min later anesthetized and perfused as described above. Frozen brains were cut at -18°C to obtain coronal sections at 30 μm. IHC was performed for both tdT and ribosomal protein S6 (S6), a cytosol protein simultaneously on floating sections containing the VTA as described above.

Quantitation of KOR translocation in VTA was performed using a method modified from Scherrer et al. (2006). Labeled brain sections were mounted in VectaShield media as described above and images were acquired with a confocal microscope (Nikon A1R) and a 60x oil objective at 0.5-μm Z-steps (voxel size = 0.21x0.21x 0.5 μm^3, 60-stacks). Measurement and calculation of KOR translocation was performed with ImageJ (Fiji version) and the workflow is detailed in Figure 8-1. Briefly, intracellular region of interest (ROI) was defined by drawing a circle with a single pixel line around the perimeter of the S6 staining, designated as circle 2. The circle 2 was uniformly enlarged by 3 pixels to define total area, designated as circle 3. The nuclear ROI was defined by DAPI staining and designated as circle 1. The ROIs were drawn on three focal planes across the Z-stack of each neuron at intervals $\geq$ 5 focal planes and registered to ROI Manager of Fiji. Background autofluorescence was corrected by the Rolling Ball (100 μm radius) algorithm of Fiji. The registered ROIs were applied to KtdT channel and the intensities of red fluorescence (KtdT) were measured for each ROI. Total receptor was defined by circle 3 minus circle 1 and cell surface receptor as circle 3 minus circle 2. The fluorescence intensity was normalized by dividing the intensity by the respective area. The results of 3 focal planes / neuron were averaged and counted as the value of one neuron. Approximately 50 neurons / mouse were measured, and the mean values were used for statistical analysis (Figure 8D). Four mice were used for each of vehicle- and U50,488H-treated groups. Image quantitation analyses were done by an observer blinded to the treatment group.

Results

Generation and characterization of a knockin mouse line expressing KtdT

We used homologous recombination to introduce tdT cDNA into exon 4 of the Oprk1 mouse gene, in frame and 5' to the stop codon (Fig. 1A). Genotyping was performed with PCR using a primer pair (Ef/Er) which detected the loxP site (95 bp) introduced 5' to the exon 4 in the KtdT allele (Fig. 1B).

Radioligand binding was conducted using the selective KOR agonist [^{3}H]U69,593 and brain membranes (1.8 mg protein/tube) prepared from wildtype (K/K), heterozygote (K/KtdT) and homozygote (KtdT/KtdT) mice. The results revealed that [^{3}H]U69,593 binding in brains was much higher in KtdT/KtdT mice than in K/K mice, with a ratio of 12:1 (Fig. 1C). Quantitative mRNA analysis revealed that a KOR mRNA ratio of 1:3.6 in the wildtype vs. KtdT/KtdT mouse brain (Fig. 1D).

Effects of the selective KOR agonist U50,488H on compound 48/80-induced scratch behavior was examined. U50,488H inhibited compound 48/80-induced scratching behavior in both KtdT/KtdT and K/K mice in dose-dependent fashion. U50,488H was about 3-time more potent in KtdT/KtdT mice (A_{50}=0.5 mg/kg) than in K/K mice (A_{50}=1.6 mg/kg) (Fig. 1E). In addition, at a dose of ~ A_{50} in anti-scratch test, U50,488H caused similar levels of hypolocomotion in KtdT/KtdT mice as in K/K mice (Fig. 1F). These results indicate that the KtdT/KtdT knockin mouse line expresses a fully functional tdTomato-tagged KOR and has intact neuronal circuitry for these behaviors. To our knowledge, this is the only tdTomato tagged G protein-coupled receptor knockin mouse reported to date. We thus used these mice to examine the distribution of KtdT in the mouse brain.

Two approaches for examination of distribution of KtdT in the mouse brain

Distribution of KtdT in the brain was examined with two approaches. The first is 3-D images of CLARITY-cleared brains without IHC staining. The second is IHC staining of brain sections with antibodies recognizing tdT. Two approaches yielded similar results.

3-D image of KtdT distribution in the mouse brain. Mouse brains were cleared with CLARITY. No IHC staining was performed. Cleared brains were imaged with confocal microscopy from dorsal side and ventral sides. Two sides were then reconstructed digitally and the 3-D image thus obtained is shown as a video clip in Movie-1. To the best of our knowledge, this is the first 3-D image of distribution of a G protein-coupled receptor in brains. Fig. 2A shows a view of a 3-D image. Fig. 2B shows an enlarged 3-D image of a portion of the brain from the SI to SNr, both of which express high levels of KtdT. Prominent KOR-tdT-containing fibers are visible in this image. Coronal sections of the 3-D image were collected digitally and shown as video clips (Movie-2). Fig. 2C are images obtained from 1-mm sections showing KtdT distribution at the cellular level in prefrontal cortex (PF), CLA, lateral septum (LS), VTA, paraventricular nucleus of thalamus (PVT), lateral habenula (LHb). Detailed KtdT distribution in the brain is described below.

IHC of KtdT showed similar distribution as that of [^{3}H]U69,593 binding to the KOR in wildtype mouse brain. We also examined KtdT distribution in conventional brain sections. As sections of un-cleared KtdT/KtdT mouse brains did not yield fluorescence of sufficiently high tdT intensity, KtdT in brain sections was detected by IHC with antibodies against the RFP, which recognized tdT. Specificity of the antibodies was examined using sections containing midbrain and cerebellum of the wildtype mice and KtdT/KtdT mice. While signals were observed in the midbrain of KtdT/KtdT mice, no fluorescent signal were detected in wildtype littermates (data not shown). There was no staining in the cerebella of KtdT/KtdT mice (data not shown), which is consistent with the finding that the mouse cerebellum does not express KOR (Slowe et al., 1999). The distribution of KtdT IHC in brain sections is similar to that of KtdT in CLARITY-cleared brains without IHC (Movie-1 and Movie-2), further demonstrating the specificity of antibody.

Autoradiography of [^{3}H]U69,593 binding to the KOR in wildtype mouse brains was performed for comparison with IHC of tdT signals in brains of KtdT/KtdT mice. As shown in Fig. 3A and 3B, the distribution of KtdT immunoreactivity is consistent with that of autoradiography of [^{3}H]U69,593 binding to the KOR in the wildtype mouse brain.

Distribution of KtdT immunoreactivity in the brain

Distribution of KtdT immunoreactivity in the brain is shown in eight coronal sections, from rostral to caudal (Fig. 3B). The greatest signal intensity was observed in the CLA, EPd, ACB shell, periaqueductal gray (PAG), and SNr. High intensity fluorescence in these regions is concordant with KOR receptor autoradiography in wildtype mice (Slowe et al., 1999). Relative intensities of KtdT in brain regions are shown in Table 1. Fig. 3C shows higher resolution images of the CLA, basolateral amygdala (BLA) and VTA as examples for high-, medium- and low-expressing brain regions, respectively.

Telencephalon

KtdT signal was seen throughout the neocortex, with the notable exception of layer IV. The most intense fluorescence in the neocortex was observed in insular and cingulate cortices, pre-bregma, as well as retrosplenial cortices, post-bregma. The CLA as well as the EPd, which borders the ventral CLA, both exhibit high-intensity signals.

Rostral limbic and olfactory regions exhibited high fluorescence, where KtdT signal was observed in the anterior olfactory nucleus, EPd, and olfactory tubercles. The dorsomedial aspect of the dorsal striatum, which comprises the CP, exhibited modest fluorescence. Strong signal was observed throughout the ventral striatum, comprising the olfactory tubercle and ACB, with distinct, high-intensity patterns of fluorescence observed in the ACB shell; however, KtdT signal was comparatively low within the ACB core. In addition, the SI exhibited high signal intensity.

KtdT signal intensity was low within the hippocampal formation, only visible within dentate gyrus regions of the hippocampus. Signal was brighter and more intense throughout other regions of the medial temporal lobe, such as the perirhinal, ectorhinal, and entorhinal cortices. Signal of moderate intensity was observed in cortical and subcortical amygdala nuclei.

Diencephalon

Low-intensity signal was observed throughout the bed nucleus of the stria terminalis, adjacent to both the dorsal and rostral aspects of the olfactory and temporal limbs of the anterior commissure. KtdT signal of varying intensity was observed throughout the rostral hypothalamus, including regions within the medial preoptic area, as well as the periventricular nucleus. Post-bregma hypothalamic signal was observed in arcuate nucleus, dorsomedial hypothalamic nucleus, lateral hypothalamic area, lateral mammillary nucleus, posterior hypothalamic area, ventral premammillary nucleus, and ventromedial hypothalamic nucleus.

KtdT signal was observed in the LHb, as well as in discrete thalamic regions, including PVT, and reuniens nucleus (RE), but KtdT signal appeared less widespread throughout the thalamus than in the hypothalamus. Low fluorescent intensity was observed in subthalamic regions including the lateral globus pallidus, subthalamic nucleus, ventrolateral geniculate nucleus, and zona incerta in these regions was low.

Mesencephalon.

KtdT signal observed in the mesencephalon was brightest in the SNr and PAG. Fluorescence was also observed in the midbrain reticular formation, most notable in the ventral tegmental area and dopamine (DA) cell group A8, also known as the retrorubral field in mice. Further midbrain staining was observed in the medial superior colliculus, as well as within the Edinger-Westphal and peripeduncular nuclei.

Pons and medulla

Staining within the lower part of the brainstem revealed striking fluorescence in several discrete raphe nuclei, including caudal linear raphe, dorsal raphe, raphe magnus, and rostral linear raphe nuclei. KtdT signal was also observed in the Barrington's nucleus, the lateral and medial parabrachial nucleus, and the rostral ventral medulla.

Co-staining of KtdT and TH in sagittal and horizontal sections of CLARITY-cleared brains

Following clearing of brains with CLARITY, some brains were cut into 1-mm sections and IHC was performed. Figs. 4A and 4C show two horizontal sections at -4.4 mm and -5.6 mm, respectively, ventral to the bregma. Figs. 5A and 5C show two sagittal sections 2.15 mm and 1.35 mm, respectively, lateral to the midline. The thickness of the sections and compilation of the confocal Z-stack images allow visualization of KtdT-containing fibers in the ACB, CP and SI that run mostly rostral-caudal direction and the dense KtdT fibers connecting the SI and SNr. This is the first observation of these KOR-containing fibers. In addition, the CLA as a contiguous band of brain structure is evident in Figs. 4C/4D.

KOR is present in some DA neurons and regulate DA neuron activities in several brain regions, including ACB (Spanagel et al., 1990; Thompson et al., 2000; Margolis et al., 2006; Morales and Margolis, 2017), which have been shown to play important roles in KOR-induced aversion (Chefer et al., 2013). TH, the rate-limiting enzyme responsible for the synthesis of catecholamines (DA, norepinephrine and epinephrine), was used as a marker for catecholamine-containing neurons.

Figs. 4B and 4D show two horizontal sections and Figs. 5B and 5D show two sagittal sections, with TH staining in green and KtdT in red. Areas of co-localization include the ACB, CP, VTA, substantia nigra pars compacta (SNc), and SNr. In contrast, the olfactory bulb and DA cell group A11 express only TH and the CLA contains only KtdT. Because of the thickness of sections and compilation of the confocal Z-stack images, TH and KtdT fibers are readily visible. Note the prominent TH fibers emanating from the VTA and SNc.

KtdT-containing fibers project from CP/ACB to SI and SNr

In Figs. 5A and 5C, prominent KtdT-expressing fiber bundles are visible in CP, ACB and SI and between SI and SNr. ISH data showed many KOR mRNA-containing neurons in CP and ACB, most co-localized with the D1 DA receptor (DRD1) or D2 DA receptor (DRD2) (Fig. 6A), indicating that KOR is expressed in D1- or D2-containing neurons. In the ventral striatum, 77% (284/371) of DRD2 cells and 91% (577/634) of DRD1 cells expressed KOR; in the dorsal striatum, 84% (569/677) of DRD2 cells and 94% (674/717) of DRD1 cells expressed KOR. Thus, most MSNs in the striatum

expressed KOR and it appears that KOR is co-localized with DRD1 to a greater extent than with DRD2. We tested the hypothesis that these KtdT fibers originate from CP and ACB and project to SI and SNr by injecting the anterograde tracer scAAV2-GFP into CP/ACB. As shown in Fig. 6C, a high level of GFP intensity was detected in the CP, ACB, and SI, which overlapped with KtdT red fluorescence to yield yellow color (Fig. 6D). In addition, GFP-containing fibers are observed projecting to the SNr (Figs. 6C and 6D). These results indicate that KtdT-containing neurons project from CP/ACB to SI and SNr.

Co-localization of KtdT and TH at the cellular level in the VTA

We then examined co-localization of KtdT and TH in the VTA at the cellular level. Fig. 7A shows KtdT staining in red, TH staining in green and merged image, which shows some yellow staining indicating likely co-localization of KtdT and TH in parts of the VTA. In the most ventral and medial portions of the VTA, KtdT staining is not overlapped with TH staining. Confocal microscopy images (Fig. 7B) show that KtdT is present mostly on cell membranes and fibers, whereas TH is located most prominently in cytosol. The merged image demonstrates localization of KtdT in some TH-immunoreactive neurons. In Movie-3  , a video of Z-stacks of confocal images facilitate identification neurons expressing both TH and KtdT. These results indicate KtdT mouse brain sections allow visualization of co-localization of KtdT and TH at the cellular level.

U50,488H induced KOR translocation in the VTA

Fig. 8A shows a coronal section containing VTA and PAG, both of which express KtdT. KtdT/KtdT mice were treated with vehicle or U50,488 (5 mg/kg, s.c.) and perfused 30 min later. In vehicle-treated mice, KtdT was present on plasma membranes, appearing as a sharp continuous thin line (Fig. 8B). Following U50,488H treatment, the KtdT surface sharp line became very dotted along with appearance of punctate staining in cytosol in many VTA neurons (Fig. 8C). The intracellular punctate staining is more visible against the green S6 staining (Fig. 8C, right panel). These results indicate that agonist treatment causes KtdT translocation from plasma membranes to intracellular

552 space. Quantitation of cell surface and intracellular KtdT revealed a significant reduction
553 in cell surface KtdT 30 min following U50,488H treatment (Fig. 8D).
554

Discussion

3-D KOR distribution in mouse brains

A combination of tagging the KOR with tdT and tissue clearing with CLARITY permitted 3-D imaging of KOR distribution in mouse brains. These are the first 3-D images of distribution of KOR and any G protein-coupled receptor in mouse brains. One advantage of conjugation of the KOR with tdT is that no IHC is necessary. IHC of cleared brains is very time consuming, often taking weeks, and requires a large amount of antibodies.

The 3-D KOR distribution was identical to that revealed by IHC of KtdT in conventional brain sections, which is similar to that of receptor autoradiography. Technical breakthroughs in brain clearing made it possible to view brain structures in 3-D. Our application of brain clearing technology proves that it is possible to study 3-D distribution of a G protein-coupled receptor, which will pave ways for more similar studies.

This mouse line also reveals for the first time a major KOR projection from ACB/CP to SI and SNr. Moreover, the KtdT mice allow visualization of KOR at the cellular level, for example, detection of co-localization of KOR with TH and receptor translocation.

The confocal microscope used in this study was not optimized for imaging cleared whole brain due to its nature of being a shared resource, which gave rise to imperfections visible as stitch-shadings in the 3D whole brain image as well as in the 1-mm section images. We are aware that the image quality could be improved with better optical hardware such as a Light Sheet microscope or a confocal microscope optimized for cleared whole brain. However, we chose to use the confocal microscope because it was readily accessible, an important consideration given the workload of the experiment. In addition, we noticed low signal/noise of the KtdT in brain, which also contributed to stitch-shadings and noises in the image because much higher laser power required exacerbated photobleaching. Increasing sampling to near Nyquist parameters did not improve shading significantly, but markedly increased image acquisition time. An extensive discussion of optical refinements is beyond the scope of this report.

CP/ACB projection to SNr expresses KOR

The high level of KtdT observed in substantia nigra is largely confined to the SNr, whereas most of DA neurons are localized in SNc, with only a small fraction of co-localization. A major KtdT-expressing neuronal fiber bundle between CP/ACB and SNr was observed. The observation of highly visible KOR-containing fibers may be due to the interaction of KOR with GEC1, a microtubule-associated protein, which facilitates transport of KOR along the neuronal fibers (Chen et al., 2006). Our anterograde tracing results demonstrated that KtdT-containing fibers project from CP/ACB to SNr. The pathways projecting from dorsomedial striatum or ACB to SNr were demonstrated previously (Soares-Cunha et al., 2016; Cheng et al., 2017); our result is the first to reveal that this pathway expresses KOR. SNr receives projections from neurons in the striatum via direct and indirect pathways (Waxman, 2017). The direct pathway originates from D1 DA receptor / dynorphin medium spiny neurons (MSNs) and exerts inhibitory effects on SNr neurons. The indirect pathway, initiating from D2 DA receptor / enkephalin MSNs, via the globus pallidus and subthalamic nucleus, exerts excitatory actions on SNr neurons. By ISH, we found that some KOR mRNA in the CP/ACB was present in D1- or D2-DA receptor-expressing neurons. Thus, it is likely that the KOR is present on both direct and indirect pathways. (Cheng et al., 2017) reported that both D1-MSNs and D2-MSNs in dorsomedial striatum are involved in alcohol consumption and KOR on these neurons may regulate their activities.

KtdT mice enabled visualization of KtdT at the cellular level

Co-Localization of KtdT with TH immunoreactivities were observed within many brain regions, particularly in limbic structures and the basal ganglia. With confocal microscopy co-localization of KtdT and TH was visualized at the cellular level (Fig. 7B). KtdT is present on plasma membranes of neuronal cell bodies and in nerve fibers, whereas TH is in cytosol. A video of Z-stack images shown in Movie-3 facilitates identification of co-localization.

KOR translocation following U50,488H administration: U50,488H caused KtdT movement into intracellular space in the VTA, which was visualized as markedly reduced cell surface KtdT and increased punctate KtdT in cytosol.

Functional neuroanatomy of the KOR

In the following sections, we briefly discuss the KOR in the brain regions and pathways known to have roles in KOR-mediated behaviors, including aversion, anxiety, addiction, pain processing and neuroendocrine functions. More importantly, we highlight several brain regions that have high KOR levels, but functions of these KORs have not been established. Possible roles of these KORs in KOR-mediated behaviors are discussed.

KOR in brain regions and pathways with identified functions for KOR

KOR in the areas involved in mood, reward, motivation and addiction: KOR was observed in the VTA, ACB, PF, anterior cingulate cortex, amygdala nuclei, bed nucleus of stria terminalis (BST) and raphe nucleus, with ACB shell exhibiting particularly intense signal. The VTA neurons project to the ACB, PF and amygdala. KOR in VTA - ACB pathway plays a critical role in aversion induced by KOR agonists and following drug abuse (Van't Veer et al., 2013; Morales and Margolis, 2017). Activation of KOR in the ACB reduces DA release and increases DA reuptake (Spanagel et al., 1990; Thompson et al., 2000), which play important roles in KOR-induced aversion (Chefer et al., 2013). Repeated stress induces dynorphin-dependent KOR activation in the BLA, ACB, dorsal raphe, and hippocampus (HIP), which is responsible for the aversive component of stress (Land et al., 2008). KOR activation in the BLA, central amygdala (CEA) and BST appear to be associated with anxiety, stress, drug and alcohol abuse and aversion associated with pain (Bruchas et al., 2009; Knoll et al., 2011; Kallupi et al., 2013; Navratilova et al., 2018). Activation of the KOR in serotoninergic neurons in the dorsal raphe nucleus – ACB pathway is responsible for KOR agonist- and stress-induced aversion and caused stress-induced drug seeking (Land et al., 2009).

KOR in Pain pathway: Moderate levels of KtdT are present in the PAG, parabrachial nucleus, some nuclei in thalamus, primary and secondary somatosensory

cortices, areas known to be involved in pain transmission and modulation. The presence of KtdT in the PAG is consistent with analgesic effects of KOR agonists (von Voigtlander et al., 1983).The spinal cord and dorsal root ganglia also express modest levels of KOR, which is outside of the scope of the current study.

KOR in Hypothalamus: KtdT is widely distributed in the hypothalamus, indicating roles of KOR in neuroendocrine functions. KOR is involved in regulation of release of hormones, such as antidiuretic hormone, luteinizing hormone, prolactin and oxytocin (Leander et al., 1985; Leadem and Yagenova, 1987; Leng et al., 1997; Butelman et al., 1999), likely through KOR in the hypothalamus.

Brain regions that have high to moderate KOR expression, but functional roles of KOR are unclear

*CLA and EP***:** The CLA and EPd have very high levels of KOR. The CLA, a long thin band-like subcortical grey matter in the forebrain, has extensive reciprocal connections with the cortex and, to lesser extents, with subcortical regions (Mathur, 2014; Wang et al., 2017). It was hypothesized to be the seat of consciousness (Crick and Koch, 2005). The EP sends extensive projections to most basal forebrain areas including the piriform, entorhinal, insular, and orbital cortices, and all cortical amygdala areas (Behan and Haberly, 1999). The EP was suggested to be an area of convergence for sensory and affect-related information and involved in aspects of the storage, consolidation, and retrieval of emotional memories (de Curtis and Pare, 2004). KOR agonists cause hallucinations and dysphoria (Pfeiffer et al., 1986; Roth et al., 2002). The KOR in the CLA and EP may be involved in KOR-mediated cognitive and perceptual effects.

PVT and RE, substructures of the midline thalamic nuclear group, show moderate levels of KtdT. PVT receives innervation from the prelimbic cortex, raphe, PAG and hypothalamus and sends projections to the ACB, amygdala, and lateral septum. Thus the PVT relays stress signals from the former to the latter (Hsu and Price, 2009) as part of a circuit that manages stress and possibly causes stress-related psychopathologies. The RE receives widespread projections from limbic and limbic-associated structures (McKenna and Vertes, 2004) and sends efferent to the

677 hippocampus, medial PF and entorhinal cortex (Wouterlood et al., 1990; Vertes, 2006).
678 These pathways are important in attentiveness and resilience to stress, among other
679 functions. Little is known about functional significance of KOR in these nuclei.
680 *LHb***:** LHb exhibited a moderate level of KtdT. LHb received inputs from forebrain
681 structures, most importantly PF, SI, globus pallidus and lateral hypothalamus. LHb
682 sends projections to DA neurons in the VTA and retromedial tegmental nucleus and
683 serotonin neurons in raphe nuclei [for reviews, see (Boulos et al., 2017; Zhou et al.,
684 2018)]. Thus, LHb connects cognitive to emotional and sensory processing (Boulos et
685 al., 2017). In animals, inhibition of LHb activity is associated with depression-like
686 behaviors and stimulation of LHb shows antidepressant-like activity [see (Yang et al.,
687 2018)]. The KOR in this brain region may play a role in depression-like behavior caused
688 by KOR activation.
689
690 **Limitations of the KtdT mouse line**
691 There are quantitative differences in KOR density in some brain regions. For
692 example, the SNr and PAG showed higher KtdT levels than expected from [^{3}H]U69,593
693 autoradiography in wildtype. In the brain, KtdT/KtdT had higher levels of KOR protein
694 and mRNA and U50,488H showed higher potency in KtdT/KtdT mice than the wildtype
695 mice. Conjugation of the KOR to tdT may affect stability and transport of the receptor.
696 As seen in the VTA (Figs. 8B & 8C), most of KtdT is present on membranes and
697 fibers and it is difficult to visualize KtdT-expressing neuronal cell bodies.
698 Counterstaining of cytosol helps, but it is often necessary to go along the Z planes of
699 confocal images to be certain (Movie-3, Fig 8-1).
700
701

References

Appleyard SM, Patterson TA, Jin WZ, Chavkin C (1997) Agonist-induced phosphorylation of the kappa-opioid receptor. J Neurochem 69:2405-2412.

Arvidsson U, Riedl M, Chakrabarti S, Vulchanova L, Lee JH, Nakano AH, Lin X, Loh HH, Law P-Y, Wessendorf MW, Elde R (1995) The kappa-opioid receptor is primarily postsynaptic: combined immunohistochemical localization of the receptor and endogenous opioids. Proc Natl Acad Sci U S A 92:5062-5066.

Behan M, Haberly LB (1999) Intrinsic and efferent connections of the endopiriform nucleus in rat. J Comp Neurol 408:532-548.

Boulos LJ, Darcq E, Kieffer BL (2017) Translating the Habenula-From Rodents to Humans. Biol Psychiatry 81:296-305.

Bruchas MR, Land BB, Chavkin C (2010) The dynorphin/kappa opioid system as a modulator of stress-induced and pro-addictive behaviors. Brain Res 1314:44-55.

Bruchas MR, Land BB, Lemos JC, Chavkin C (2009) CRF1-R activation of the dynorphin/kappa opioid system in the mouse basolateral amygdala mediates anxiety-like behavior. PLoS One 4:e8528.

Butelman ER, Harris TJ, Kreek MJ (1999) Effects of E-2078, a stable dynorphin A(1-8) analog, on sedation and serum prolactin levels in rhesus monkeys. Psychopharmacology (Berlin) 147:73-80.

Carlezon WA, Jr., Beguin C, Knoll AT, Cohen BM (2009) Kappa-opioid ligands in the study and treatment of mood disorders. Pharmacol Ther 123:334-343.

Carr GV, Bangasser DA, Bethea T, Young M, Valentino RJ, Lucki I (2010) Antidepressant-like effects of kappa-opioid receptor antagonists in Wistar Kyoto rats. Neuropsychopharmacology 35:752-763.

Chefer VI, Backman CM, Gigante ED, Shippenberg TS (2013) Kappa opioid receptors on dopaminergic neurons are necessary for kappa-mediated place aversion. Neuropsychopharmacology 38:2623-2631.

Chen C, Li JG, Chen Y, Huang P, Wang Y, Liu-Chen LY (2006) GEC1 interacts with the kappa opioid receptor and enhances expression of the receptor. J Biol Chem 281:7983-7993.

733 Cheng Y, Huang CCY, Ma T, Wei X, Wang X, Lu J, Wang J (2017) Distinct Synaptic
734 Strengthening of the Striatal Direct and Indirect Pathways Drives Alcohol
735 Consumption. Biol Psychiatry 81:918-929.
736 Chung K, Deisseroth K (2013) CLARITY for mapping the nervous system. Nat Methods
737 10:508-513.
738 Chung K, Wallace J, Kim SY, Kalyanasundaram S, Andalman AS, Davidson TJ,
739 Mirzabekov JJ, Zalocusky KA, Mattis J, Denisin AK, Pak S, Bernstein H,
740 Ramakrishnan C, Grosenick L, Gradinaru V, Deisseroth K (2013) Structural and
741 molecular interrogation of intact biological systems. Nature 497:332-337.
742 Cowan A, Kehner GB, Inan S (2015) Targeting Itch with Ligands Selective for kappa
743 Opioid Receptors. Handb Exp Pharmacol 226:291-314.
744 Crick FC, Koch C (2005) What is the function of the claustrum? Philos Trans R Soc
745 Lond B Biol Sci 360:1271-1279.
746 de Curtis M, Pare D (2004) The rhinal cortices: a wall of inhibition between the
747 neocortex and the hippocampus. Prog Neurobiol 74:101-110.
748 Drake CT, Patterson TA, Simmons ML, Chavkin C, Milner TA (1996) Kappa opioid
749 receptor-like immunoreactivity in guinea pig brain: ultrastructural localization in
750 presynaptic terminals in hippocampal formation. J Comp Neurol 370:377-395.
751 Erbs E, Faget L, Scherrer G, Matifas A, Filliol D, Vonesch JL, Koch M, Kessler P,
752 Hentsch D, Birling MC, Koutsourakis M, Vasseur L, Veinante P, Kieffer BL,
753 Massotte D (2015) A mu-delta opioid receptor brain atlas reveals neuronal co-
754 occurrence in subcortical networks. Brain Struct Funct 220:677-702.
755 Hsu DT, Price JL (2009) Paraventricular thalamic nucleus: subcortical connections and
756 innervation by serotonin, orexin, and corticotropin-releasing hormone in macaque
757 monkeys. J Comp Neurol 512:825-848.
758 Huang P, Chiu YT, Chen C, Wang Y, Liu-Chen LY (2013) A G protein-coupled receptor
759 (GPCR) in red: live cell imaging of the kappa opioid receptor-tdTomato fusion
760 protein (KOPR-tdT) in neuronal cells. J Pharmacol Toxicol Methods 68:340-345.
761 Kallupi M, Wee S, Edwards S, Whitfield TW, Jr., Oleata CS, Luu G, Schmeichel BE,
762 Koob GF, Roberto M (2013) Kappa opioid receptor-mediated dysregulation of

763 gamma-aminobutyric acidergic transmission in the central amygdala in cocaine
764 addiction. Biol Psychiatry 74:520-528.
765 Kamimura K, Yokoo T, Kamimura H, Sakamaki A, Abe S, Tsuchiya A, Takamura M,
766 Kawai H, Yamagiwa S, Terai S (2017) Long-term efficacy and safety of
767 nalfurafine hydrochloride on pruritus in chronic liver disease patients: Patient-
768 reported outcome based analyses. PLoS One 12:e0178991.
769 Kim SY, Cho JH, Murray E, Bakh N, Choi H, Ohn K, Ruelas L, Hubbert A, McCue M,
770 Vassallo SL, Keller PJ, Chung K (2015) Stochastic electrotransport selectively
771 enhances the transport of highly electromobile molecules. Proc Natl Acad Sci U
772 S A 112:E6274-6283.
773 Knoll AT, Muschamp JW, Sillivan SE, Ferguson D, Dietz DM, Meloni EG, Carroll FI,
774 Nestler EJ, Konradi C, Carlezon WA, Jr. (2011) Kappa opioid receptor signaling
775 in the basolateral amygdala regulates conditioned fear and anxiety in rats. Biol
776 Psychiatry 70:425-433.
777 Land BB, Bruchas MR, Lemos JC, Xu M, Melief EJ, Chavkin C (2008) The dysphoric
778 component of stress is encoded by activation of the dynorphin kappa-opioid
779 system. J Neurosci 28:407-414.
780 Land BB, Bruchas MR, Schattauer S, Giardino WJ, Aita M, Messinger D, Hnasko TS,
781 Palmiter RD, Chavkin C (2009) Activation of the kappa opioid receptor in the
782 dorsal raphe nucleus mediates the aversive effects of stress and reinstates drug
783 seeking. Proc Natl Acad Sci U S A 106:19168-19173.
784 Leadem CA, Yagenova SV (1987) Effects of specific activation of mu-, delta- and
785 kappa-opioid receptors on the secretion of luteinizing hormone and prolactin in
786 the ovariectomized rat. Neuroendocrinology 45:109-117.
787 Leander JD, Zerbe RL, Hart JC (1985) Diuresis and suppression of vasopressin by
788 kappa opioids: comparison with mu and delta opioids and clonidine. J Pharmacol
789 Exp Ther 234:463-469.
790 Leng G, Dye S, Bicknell RJ (1997) Kappa-opioid restraint of oxytocin secretion:
791 plasticity through pregnancy. Neuroendocrinology 66:378-383.
792 Liu JJ, Chiu YT, DiMattio KM, Chen C, Huang P, Gentile TA, Muschamp JW, Cowan A,
793 Mann M, Liu-Chen LY (2019) Phosphoproteomic approach for agonist-specific

signaling in mouse brains: mTOR pathway is involved in kappa opioid aversion. Neuropsychopharmacology 44:939-949.

Liu Y, Keefe K, Tang X, Lin S, Smith GM (2014) Use of self-complementary adeno-associated virus serotype 2 as a tracer for labeling axons: implications for axon regeneration. PLoS One 9:e87447.

Mansour A, Khachaturian H, Lewis ME, Akil H, Watson SJ (1988) Anatomy of CNS opioid receptors. Trends Neurosci 11:308-314.

Mansour A, Burke S, Pavlic RJ, Akil H, Watson SJ (1996) Immunohistochemical localization of the cloned kappa 1 receptor in the rat CNS and pituitary. Neuroscience 71:671-690.

Margolis EB, Lock H, Chefer VI, Shippenberg TS, Hjelmstad GO, Fields HL (2006) Kappa opioids selectively control dopaminergic neurons projecting to the prefrontal cortex. Proc Natl Acad Sci U S A 103:2938-2942.

Mathur BN (2014) The claustrum in review. Front Syst Neurosci 8:48.

McKenna JT, Vertes RP (2004) Afferent projections to nucleus reuniens of the thalamus. J Comp Neurol 480:115-142.

McLaughlin JP, Marton-Popovici M, Chavkin C (2003) Kappa opioid receptor antagonism and prodynorphin gene disruption block stress-induced behavioral responses. J Neurosci 23:5674-5683.

McLaughlin JP, Land BB, Li S, Pintar JE, Chavkin C (2006) Prior activation of kappa opioid receptors by U50,488 mimics repeated forced swim stress to potentiate cocaine place preference conditioning. Neuropsychopharmacology 31:787-794.

Michel MC, Wieland T, Tsujimoto G (2009) How reliable are G-protein-coupled receptor antibodies? Naunyn Schmiedebergs Arch Pharmacol 379:385-388.

Morales M, Margolis EB (2017) Ventral tegmental area: cellular heterogeneity, connectivity and behaviour. Nat Rev Neurosci 18:73-85.

Nakao K, Mochizuki H (2009) Nalfurafine hydrochloride: a new drug for the treatment of uremic pruritus in hemodialysis patients. Drugs Today (Barc) 45:323-329.

Navratilova E, Ji G, Phelps C, Qu C, Hein M, Yakhnitsa V, Neugebauer V, Porreca F (2018) Kappa opioid signaling in the central nucleus of the amygdala promotes disinhibition and aversiveness of chronic neuropathic pain. Pain.

825 Ozawa A, Brunori G, Mercatelli D, Wu J, Cippitelli A, Zou B, Xie XS, Williams M, Zaveri
826 NT, Low S, Scherrer G, Kieffer BL, Toll L (2015) Knock-In Mice with NOP-eGFP
827 Receptors Identify Receptor Cellular and Regional Localization. J Neurosci
828 35:11682-11693.
829 Paxinos G, Franklin KBJ (1997) The Mouse Brain in Stereotaxic Coodinates Deluxe
830 Edition of the Atlas, Second Edition Edition: Academic Press.
831 Pfeiffer A, Brantl V, Herz A, Emrich HM (1986) Psychotomimesis mediated by kappa
832 opiate receptors. Science 233:774-776.
833 Roth BL, Baner K, Westkaemper R, Siebert D, Rice KC, Steinberg S, Ernsberger P,
834 Rothman RB (2002) Salvinorin A: a potent naturally occurring nonnitrogenous
835 kappa opioid selective agonist. Proc Natl Acad Sci U S A 99:11934-11939.
836 Scherrer G, Tryoen-Toth P, Filliol D, Matifas A, Laustriat D, Cao YQ, Basbaum AI,
837 Dierich A, Vonesh JL, Gaveriaux-Ruff C, Kieffer BL (2006) Knockin mice
838 expressing fluorescent delta-opioid receptors uncover G protein-coupled receptor
839 dynamics in vivo. Proc Natl Acad Sci U S A 103:9691-9696.
840 Shippenberg TS, Zapata A, Chefer VI (2007) Dynorphin and the pathophysiology of
841 drug addiction. Pharmacol Ther 116:306-321.
842 Simonin F, Valverde O, Smadja C, Slowe S, Kitchen I, Dierich A, Le M, Roques BP,
843 Maldonado R, Kieffer BL (1998) Disruption of the kappa-opioid receptor gene in
844 mice enhances sensitivity to chemical visceral pain, impairs pharmacological
845 actions of the selective kappa-agonist U-50,488H and attenuates morphine
846 withdrawal. EMBO Journal 17:886-897.
847 Slowe SJ, Simonin F, Kieffer B, Kitchen I (1999) Quantitative autoradiography of mu-
848 ,delta- and kappa1 opioid receptors in kappa-opioid receptor knockout mice.
849 Brain Res 818:335-345.
850 Soares-Cunha C, Coimbra B, Sousa N, Rodrigues AJ (2016) Reappraising striatal D1-
851 and D2-neurons in reward and aversion. Neuroscience and biobehavioral
852 reviews 68:370-386.
853 Spanagel R, Herz A, Shippenberg TS (1990) The effects of opioid peptides on
854 dopamine release in the nucleus accumbens: an in vivo microdialysis study. J
855 Neurochem 55:1734-1740.

856 Thompson AC, Zapata A, Justice JB, Jr., Vaughan RA, Sharpe LG, Shippenberg TS
857 (2000) Kappa-opioid receptor activation modifies dopamine uptake in the nucleus
858 accumbens and opposes the effects of cocaine. J Neurosci 20:9333-9340.
859 Tomer R, Ye L, Hsueh B, Deisseroth K (2014) Advanced CLARITY for rapid and high-
860 resolution imaging of intact tissues. Nat Protoc 9:1682-1697.
861 Unterwald EM, Knapp C, Zukin RS (1991) Neuroanatomical localization of kappa 1 and
862 kappa 2 opioid receptors in rat and guinea pig brain. Brain Res 562:57-65.
863 Van't Veer A, Bechtholt AJ, Onvani S, Potter D, Wang Y, Liu-Chen LY, Schutz G,
864 Chartoff EH, Rudolph U, Cohen BM, Carlezon WA, Jr. (2013) Ablation of Kappa-
865 Opioid Receptors from Brain Dopamine Neurons has Anxiolytic-Like Effects and
866 Enhances Cocaine-Induced Plasticity. Neuropsychopharmacology 38:1585-1597.
867 Vertes RP (2006) Interactions among the medial prefrontal cortex, hippocampus and
868 midline thalamus in emotional and cognitive processing in the rat. Neuroscience
869 142:1-20.
870 von Voigtlander PF, Lahti RA, Ludens JH (1983) U-50,488: a selective and structurally
871 novel non-Mu (kappa) opioid agonist. J Pharmacol Exp Ther 224:7-12.
872 Wang Q, Ng L, Harris JA, Feng D, Li Y, Royall JJ, Oh SW, Bernard A, Sunkin SM, Koch
873 C, Zeng H (2017) Organization of the connections between claustrum and cortex
874 in the mouse. J Comp Neurol 525:1317-1346.
875 Wang YJ, Rasakham K, Huang P, Chudnovskaya D, Cowan A, Liu-Chen LY (2011) Sex
876 difference in ê-opioid receptor (KOPR)-mediated behaviors, brain region KOPR
877 level and KOPR-mediated guanosine 5'-O-(3-[35S]thiotriphosphate) binding in
878 the guinea pig. J Pharmacol Exp Ther 339:438-450.
879 Waxman SG (2017) Control of Movement. In: Clinical Neuroanatomy. New York, NY:
880 McGraw-Hill
881 Wee S, Koob GF (2010) The role of the dynorphin-kappa opioid system in the
882 reinforcing effects of drugs of abuse. Psychopharmacology (Berl) 210:121-135.
883 Wouterlood FG, Saldana E, Witter MP (1990) Projection from the nucleus reuniens
884 thalami to the hippocampal region: light and electron microscopic tracing study in
885 the rat with the anterograde tracer Phaseolus vulgaris-leucoagglutinin. J Comp
886 Neurol 296:179-203.

887 Xu W, Wang Y, Ma Z, Chiu YT, Huang P, Rasakham K, Unterwald E, Lee DY, Liu-Chen
888 LY (2013) l-Isocorypalmine reduces behavioral sensitization and rewarding
889 effects of cocaine in mice by acting on dopamine receptors. Drug Alcohol
890 Depend 133:693-703.
891 Yang Y, Wang H, Hu J, Hu H (2018) Lateral habenula in the pathophysiology of
892 depression. Curr Opin Neurobiol 48:90-96.
893 Zhou T, Sandi C, Hu H (2018) Advances in understanding neural mechanisms of social
894 dominance. Curr Opin Neurobiol 49:99-107.

895
896

Figure legends

Figure 1. Generation and characterization of KOR-tdTomato (KtdT/KtdT) knockin mice and comparison with the wild KOR (K/K) mice.

(A) Targeting strategy. *Oprk1* exons 3 and 4, tdTomato cDNA, and the floxed neomycin cassette are shown as empty, gray, and black boxes, respectively. Homologous recombination (HR) was followed by Cre recombinase treatment (Cre) in ES cells.

(B) Genotyping by PCR analysis using primer pair Ef/Er as shown in (A) and genomic DNA from mouse ears as templates.

(C) [^{3}H]U69,593 binding (dpm) to receptor in mouse whole brain membranes (1.8 mg protein) was performed with 4.5 nM [^{3}H]U69,593 and non-specific binding was determined by naloxone (10 μM). Data are mean ± SEM (n=4).

(D) Receptor mRNA levels were determined by real-time qRT-PCR with RNA preparations from mouse whole brains. Data are mean ± SEM (K/K, n=4; KtdT/KtdT, n=3). **P <0.01 and ***P< 0.001, compared with the wildtype (K/K) by two-tailed Student's *t* test.

(E) U50,488H inhibited scratching behavior induced by compound 48/80 in both KtdT/KtdT and K/K mice. Male mice were pretreated s.c. with saline or U50,488 (0.2-5 mg/kg) and 20 min later, compound 48/80 was injected into the nape of the neck and bouts of scratching were counted for 30 min and normalized to the saline group of each mouse strain. Each value represents mean ± SEM (n=10).

(F) U50,488H inhibited novelty-induced locomotor activities in both KtdT/KtdT and K/K mice. Male mice were treated s.c. with saline or U50,488H (at doses of A50 values in the anti-scratching test) and put into locomotor chambers right after injections. Total locomotor activities (breaks of infrared beams) were continuously monitored using a Digiscan D Micro System over a 90-min period. Cumulative data between 20 and 50 min post-injection are shown here. Each value represents mean ± SEM (n=8). Data were analyzed by 2-way ANOVA followed by Tukey's post-hoc test. * $p < 0.05$, compared with the respective saline group.

928 **Figure 2 (A) A 3-D image of mouse brain cleared with CLARITY showing brain-**
929 **wide distribution of KtdT**. The 3D whole brain image was reconstructed from ventral
930 and dorsal stacks acquired separately with optical settings described in Methods and
931 Materials. Directions: Anterior (A), Posterior (P), Ventral (V), Dorsal (D), lateral (L),
932 Medial (M). The autofluorescence in green channel was used as a reference (Ref) to
933 whole brain volume which is pseudo-colored in cyan. Experiments were performed on
934 three brains with similar results. See Movie-1 and Movie-2 for video clips.
935 **(B)** An enlarged view of a portion of the 3-D image showing prominent KtdT fiber
936 bundles between SI and SNr.
937 **(C)** Images (I-V) were presented as optical sections from 1-mm coronal blocks of mouse
938 brains showing KtdT neurons in the prefrontal cortex (PFC), claustrum (CLA), lateral
939 septum (LS), ventral tegmental area (VTA), paraventricular nucleus of thalamus (PVT),
940 lateral habenula (LHb). The brain region of the images is marked by circles in the
941 horizontal view of 3D rendering (grey).
942
943 **Figure 3. (A) Comparison of IHC staining of KtdT (top row) with autoradiography**
944 **of [^{3}H]U69,593 binding to the KOR (bottom row) in two coronal brain sections** (30
945 μm for IHC and 20 μm for autoradiography in thickness)**.** IHC images of KtdT were
946 captured with a wide field fluorescence microscope. Experiments were performed on
947 three brains each with similar results.
948 **(B) Distribution of KtdT in coronal brain sections.** IHC images of KtdT were
949 captured with a wide field fluorescence microscope. Rostral-caudal coordinates in
950 reference to bregma are indicated. The numbers in parenthesis are the coronal section
951 numbers in the Mouse Atlas of Allen Brain Institute.
952 (https://mouse.brain-map.org/experiment/thumbnails/100048576?image_type=atlas)
953 Experiments were performed on three brains each with similar results. For
954 neuroanatomical sites, see list of abbreviations for brain nucleus and regions.
955 **(C) Three higher resolution images with relative intensities from high to low.** The
956 images were taken with 20X objective on confocal microscope. The region CLA, BLA
957 and VTA were chosen as representatives of high to low KtdT expression levels.
958

List of abbreviations for brain nucleus and regions [per Mouse Brain Atlas of Allen Brain Institute (https://mouse.brain-map.org/experiment/thumbnails/100048576?image_type=atlas)]
A11: A11 dopamine neurons; aco: anterior commissure; AC: anterior cingulate cortex; ACB: nucleus accumbens; alv: alveus of hippocampus; ARH: arcuate nucleus of hypothalamus; BLA: basolateral amygdala nucleus; BMA: basomedial amygdala nucleus; BST: bed nucleus of the stria terminalis; CB: cerebellum; CEA: central amygdalar nucleus; CLA: claustrum; CP: caudate putamen; CS: superior central nucleus raphe; CTX: cortex; ECT: ectorhinal cortex; ENT: entorhinal cortex; EP: endopiriform nucleus; EPd: dorsal endopiriform nucleus; DMH: dorsomedial nucleus of the hypothalamus; DR: dorsal raphe nucleus; EW: Edinger-Westphal nucleus; Hb: habenula; HIP: hippocampus; LA: lateral amygdalar nucleus; LHb: lateral habenula; LM: lateral mammillary nucleus; MEA: medial amygdalar nucleus; MM: Medial mammary nucleus; MPO: medial preoptic area; nst: nigrostriatal tract; OB: olfactory bulb; OT: olfactory tubercle; PAG: periaqueductal gray; PER: perirhinal cortex; PF: prefrontal cortex; PH: posterior hypothalamic area; PVH: paraventricular hypothalamus nucleus; PVT: paraventricular nucleus of thalamus; RE: reuniens nucleus of thalamus; RSP: retrosplenial cortex; SI: substantia innominata; SNc: substantia nigra, pars compacta; SNr: substantia nigra, pars reticulata; st: stria terminalis; STN: subthalamic nucleus; SC: superior colliculus; VTA: ventral tegmental area

Figure 4. A thick horizontal brain section (1 mm) of the KtdT mouse showing IHC staining of (A) KtdT (red) alone and (B) both KtdT (red) and TH (green). KtdT/KtdT mice were perfused and cleared with the CLARITY method. Cleared brains were sectioned at 1 mm with a Vibratome and IHC was performed on floating sections for TH and KtdT. IHC image Z-stacks were captured with a confocal microscope and the tiles were stitched in real time with NIS-Element software. The images shown are maximum intensity projection (MaxIP) of the stacks to demonstrate long range projections. In these images, TH- or KtdT-containing fibers are clearly visible between substantia nigra (SN) and caudate putamen (CP).
(A, B) This section is approximately -4.4 mm ventral to Bregma
(C, D) This section is approximately -5.6 mm ventral to Bregma.

Figure 5. A sagittal brain section (1 mm) of the KtdT mouse showing IHC staining of (A) KtdT (red) alone and (B) both KtdT (red) and tyrosine hydroxylase (green). See Fig. 4 Legend. Note that nerve fibers are clearly visible.

(A, B) This section is approximately 2.15 mm lateral to the midline.
(C, D) This section is approximately 1.35 mm lateral to the midline.

Figure 6. Anterograde tracing shows projection of KtdT-containing neurons from caudate putamen (CP) and nucleus accumbens (ACB) to substantia innominata (SI) and substantia nigra pars reticulata (SNr).
(A) ISH of KOR mRNA: Wildtype C57BL/6N mice were used. ISH was performed with RNAscope on coronal brain sections at regions containing CP and ACB. Experiments were performed on three brains with similar results. Some KOR mRNA (red) is present in D1 (green) or D2 (white) DA receptor-expressing neurons.
(B, C, D) Anterograde tracing from CP and ACB. Adult KtdT/KtdT mice were injected with scAAV2-GFP tracer (0.2 μl) into the CP and ACB. Three to 4 weeks after injection, mice were perfused, cleared with CLARITY, processed for KtdT IHC on 1-mm sagittal sections and confocal microscopy as described in Fig. 4 legend. (B) Red: KtdT; (C) Green: scAAV2-GFP; (D) Red + Green + Blue (DAPI). Yellow color indicates overlap of KtdT and scAAV2-GFP. The results indicate projections from CP and ACB to SI and SNr. The experiment was performed three times with similar results.

Figure 7. Double IHC staining of KtdT (red) and TH (green) in the ventral tegmental area (VTA). IHC staining for KtdT (red) and TH (green) was performed on coronal sections 30 μm) containing the VTA.
(A) The three figure show macro views of the VTA region with a 4x objective on a wide-field fluoresce microscope.
(B) The two figures show KtdT and TH staining acquired with a NikonA1R confocal microscope and a 60x objective, each of which is a MaxIP of three focal planes from a Z-stack. Co-localization of both in some neurons are indicated by arrows. The Z stacks of confocal images are shown as a video in Movie-3.

Figure 8. U50,488 induced KOR translocation into cells in the VTA. KtdT/KtdT mice were injected s.c. with the agonist U50,488 at 5 mg/kg or vehicle (n=4 each). Thirty min later, mice were anesthetized and perfused and coronal sections containing the VTA

were processed for IHC for KtdT (red) and ribosomal protein S6 used to define cytosol space (green).

(A) Macro view of the region containing VTA and PAG. The image was acquired with a 10X objective on confocal microscope. The dotted circles define the area where KtdT neurons were selected for analysis.

(B) Vehicle group: KtdT in VTA neurons (marked by arrows) are clearly observed as red sharp outlines (most likely in cell membranes). The image is a single focal plane of a Z-stack acquired with a 60X objective on confocal microscope.

(C) U50,488 group: The image was obtained similarly as in **(B).** Note that U50,488-induced KtdT translocation in KtdT neurons are evidenced by simultaneously exhibiting broken and dotted KtdT surface outlines and punctate staining in cytosol space as contrasted by S6 staining.

(D) KtdT translocation was quantified with the method described in Figure 8-1 and shown as graph. Each value represents mean ± SEM (n=4). Data were analyzed with Student's *t*-test. **** $p<0.0001$.

Extended data

Movie-1. A video clip of 3-D images of KtdT/KtdT mouse brains showing KtdT distribution. Adult KtdT/KtdT mice were perfused and brains were cleared via CLARITY. Brains were imaged without IHC from dorsal and ventral sides and images were digitally re-constructed into 3-D images. Experiments were performed on three brains with similar results.

Movie-2. A video clip of optical coronal sections of KtdT/KtdT mouse brains showing KtdT distribution. See Movie-1 legend. Coronal sections were obtained digitally and are shown as video clips. Experiments were performed on three brains with similar results.

Movie-3. A video clip of Z-stacks of confocal images of a VTA section co-stained for KtdT (red), TH (green) and DAPI (blue). Experiments were performed on five VTAs with similar results.

Figure 8-1. Workflow for quantitation of KOR translocation. A 5-step procedure was applied. **Identify**, orthogonal view moving across Z-stack was used to select and confirm KtdT positive neurons (see Movie-3); **Tracing**, S6 protein and DAPI markers were used for unbiased and KtdT activity-independent tracing, three planes/neuron were traced due to the anisotropic nature of KtdT neurons; **Register,** multi-plane region of interests (ROIs) were added in ROI manager; **Measure,** apply all defined ROIs to KtdT channel, obtain data of intensities and go to **Calculation** next.

Figure 1

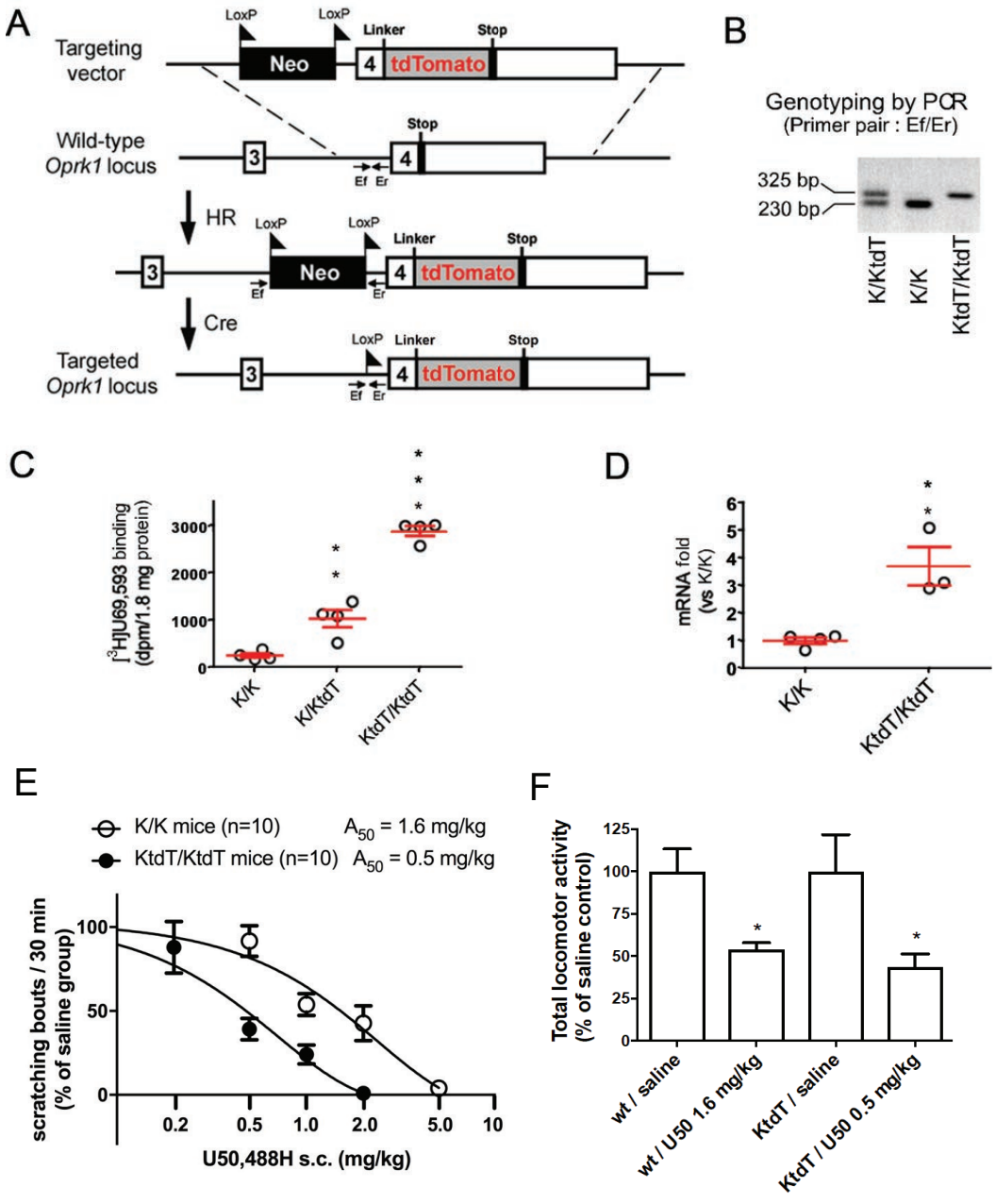

Figure 2

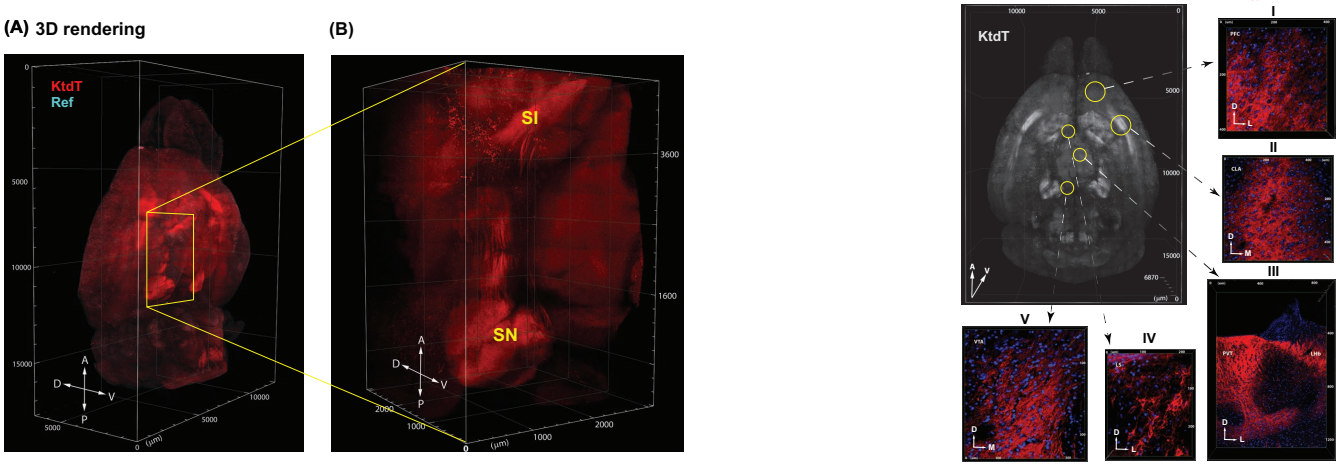

Figure 3

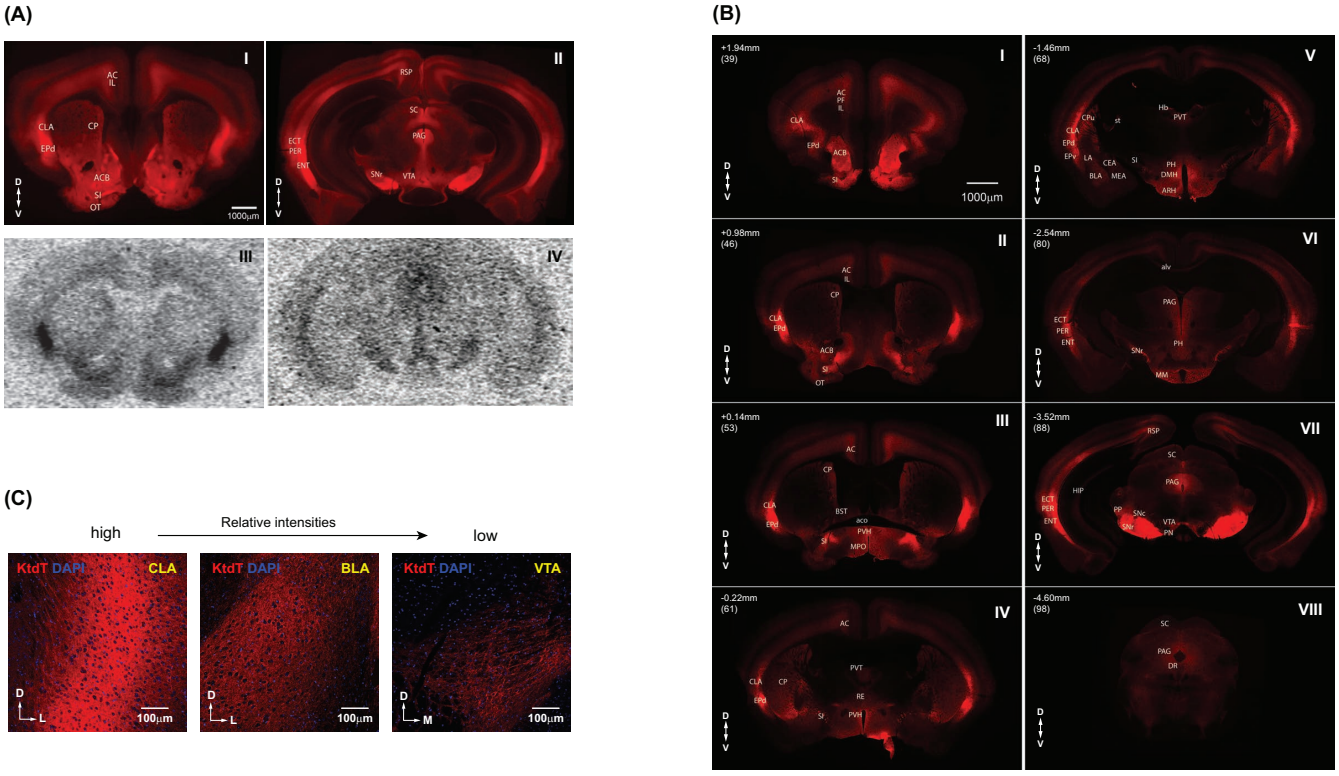

Figure 4

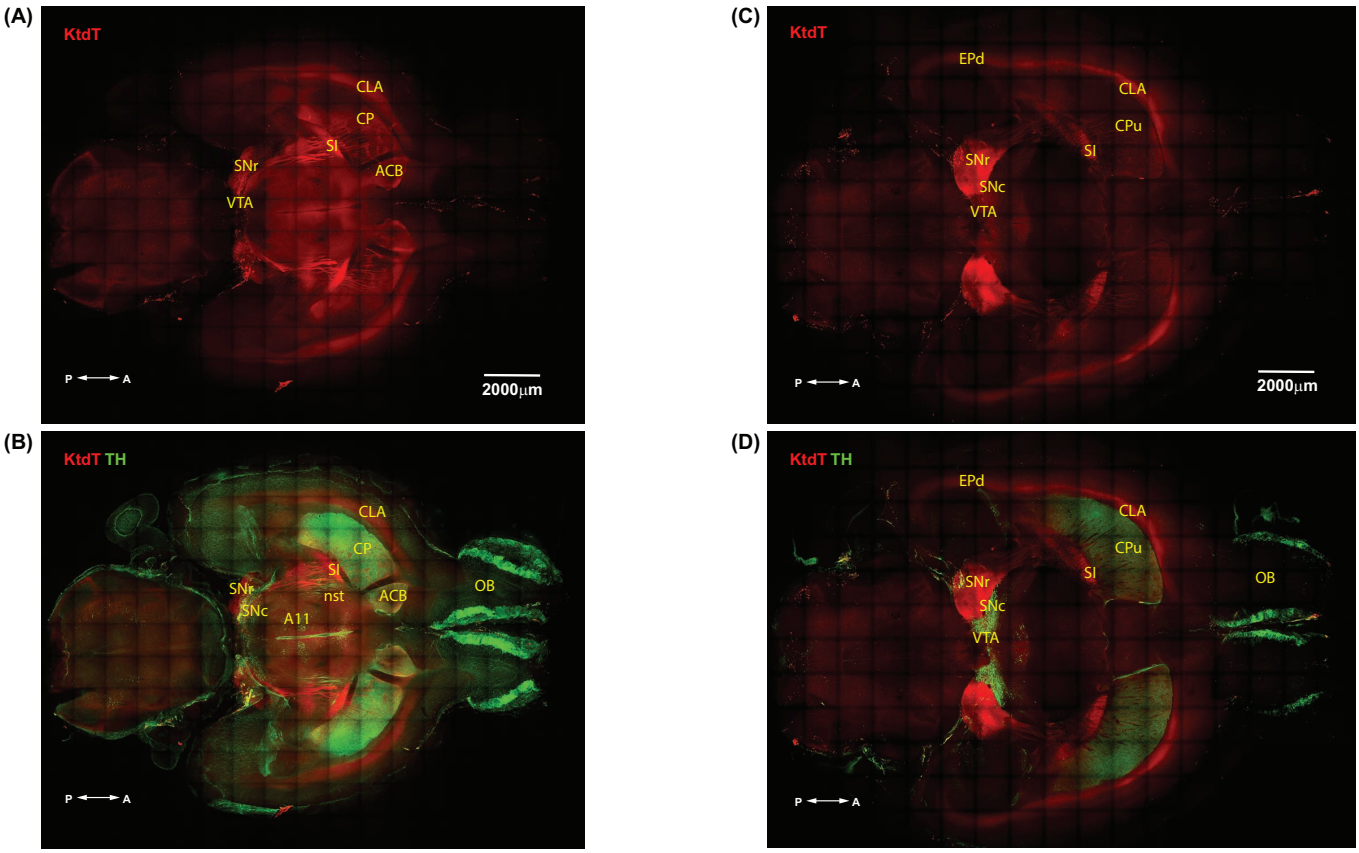

Figure 5

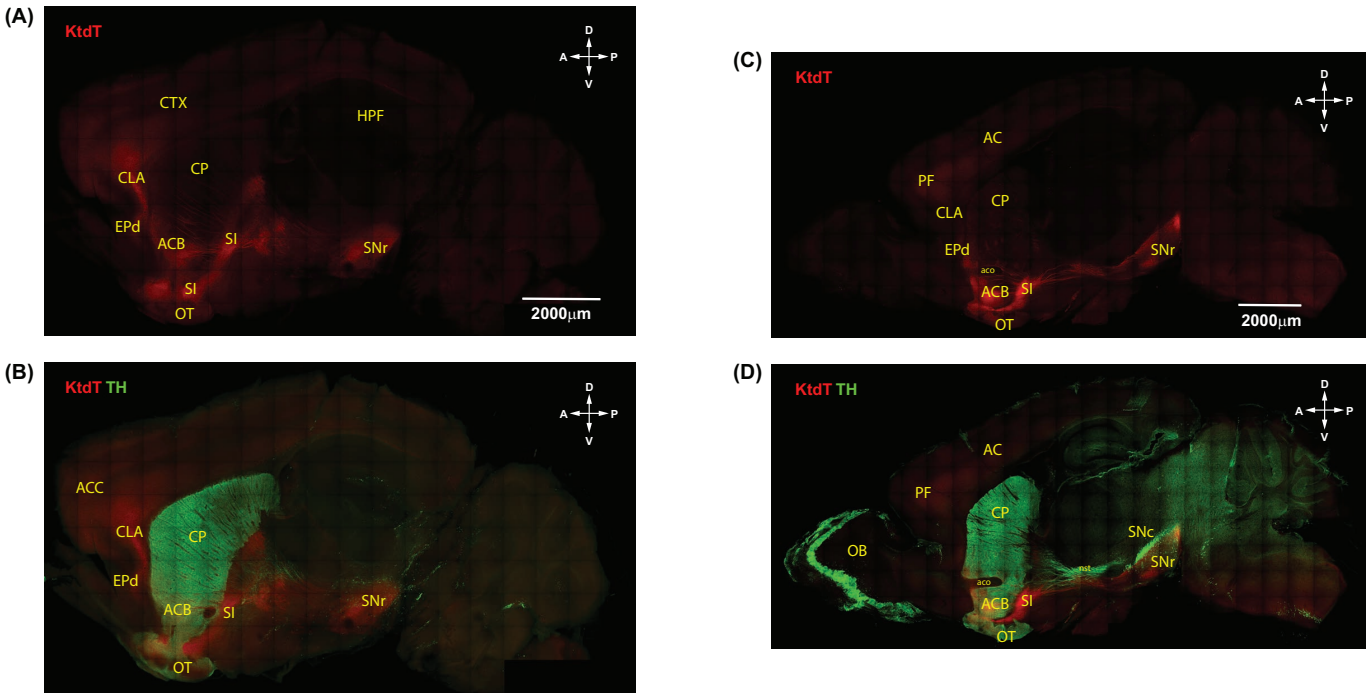

Figure 6

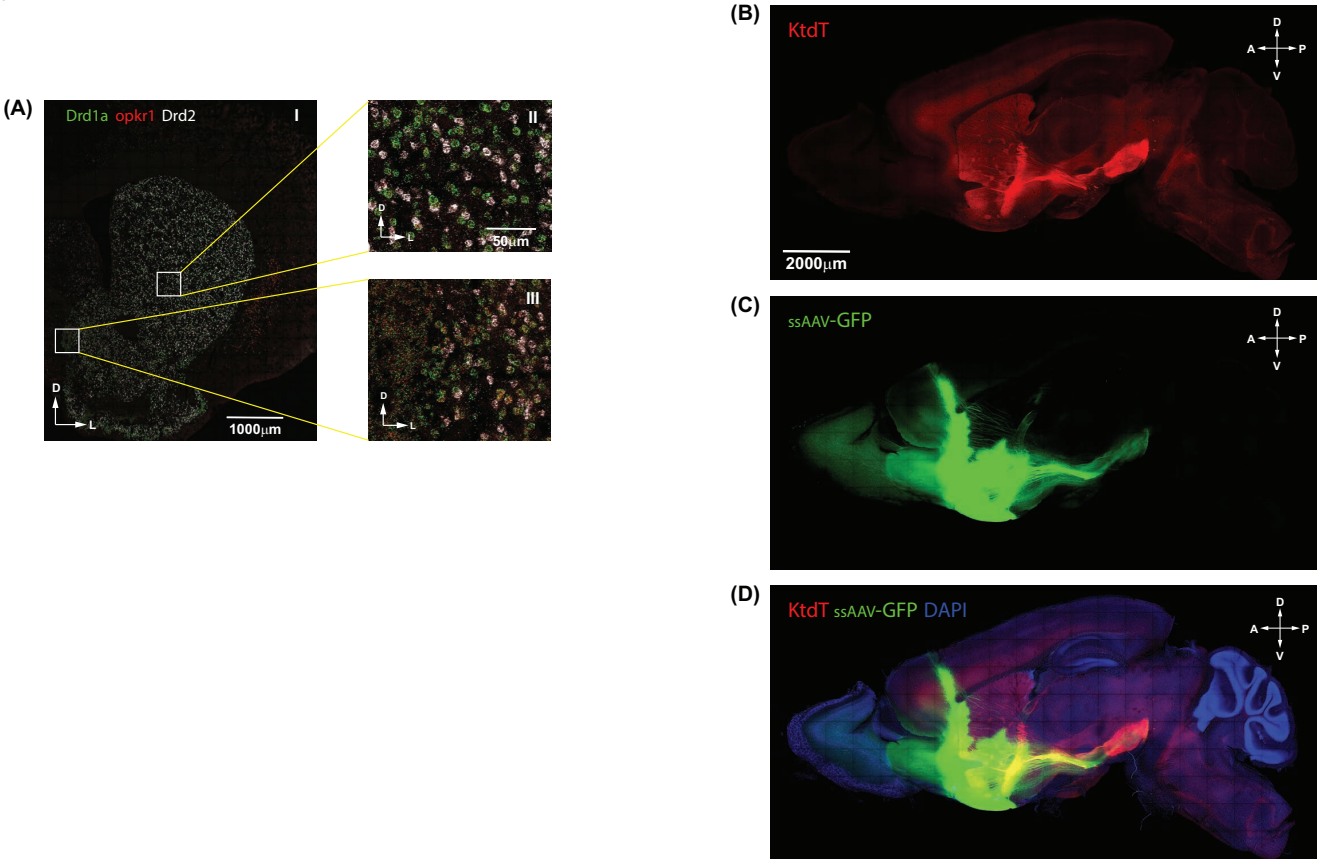

Figure 7

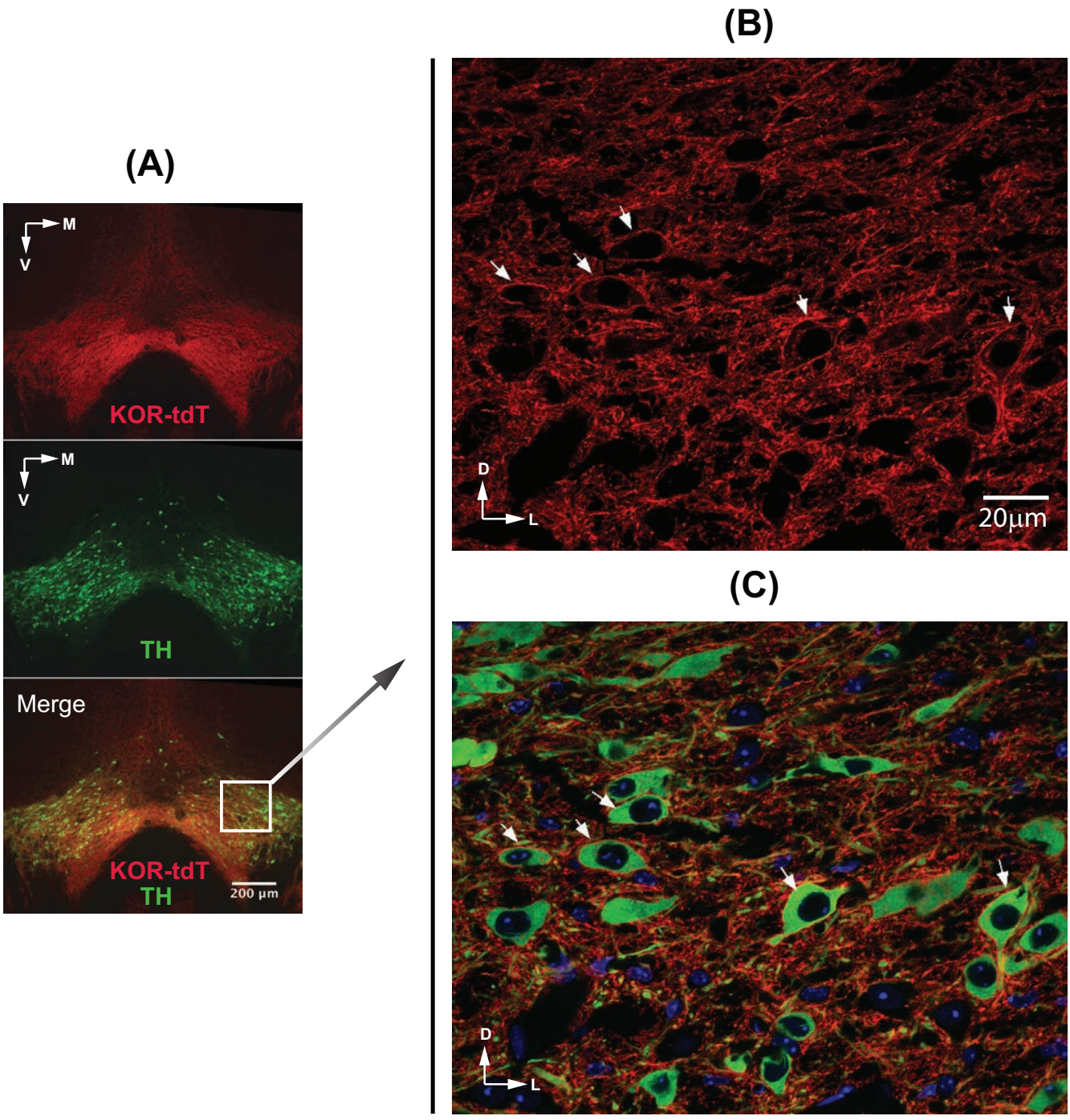

Figure 8

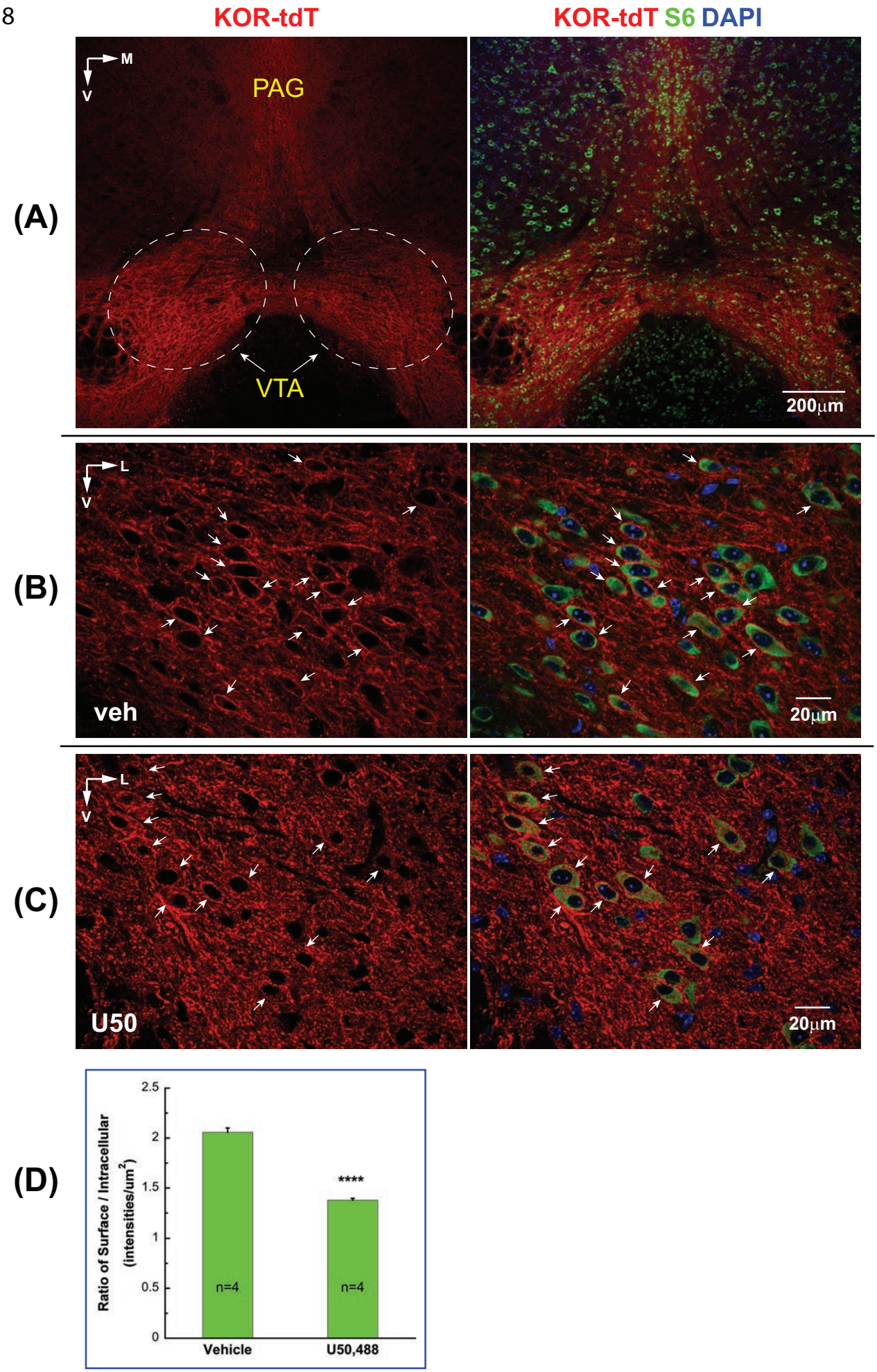

Table 1. KOR distribution in brain regions of KtdT/KtdT mice. 4 indicates the highest density and 1 the lowest. Data are derived from 3 mice.

Telencephalon	
Amygdala	
Central nucleus	1
Cortical nucleus	1
Basolateral nucleus	2
Medial nucleus	1
Bed nucleus, stria terminalis	1
Cerebral Cortex	
Layer 1	1
Layer 2/3	2
Layer 4	0
Layer 5	2
Layer 6	2
Claustrum	4
Caudate-Putamen	1
Endopiriform nucleus	4
Globus pallidus	1
Hippocampal formation	
Cornu ammonis	1
Dentate gyrus	1
Septum	
Lateral septum	1
Medial septum	1
Substantia innominata	3
Ventral striatum	
Nucleus accumbens core	2
Nucleus accumbens Shell	3
Olfactory tubercle	2
Diencephalon	
Epithalamus	
Lateral habenula	1
Medial habenula	1
Hypothalamus	
Arcuate nucleus	2
Dorsomedial nucleus	3
Lateral hypothalamic area	1
Mammillary nucleus	1
Paraventricular nucleus	2
Periventricular area	3
Preoptic area	1
Suprachiasmatic nucleus	2
Retrochiasmatic nucleus	2
Subthalamus	
Substantia innominata	2
Subthalamic nucleus	2
Zona incerta	1
Thalamus	
Periventricular nucleus	2
Reuniens nucleus	1
Mesencephalon	
Edinger-Westphal nucleus	2
Periaqueductal gray	3
Substantia nigra	
pars compacta	1
pars reticulata	4
Superior Colliculus	3
Retrorubral field (A8)	3
Ventral tegmental area	2
pons / medulla	
Nucleus raphe magnus	3
Parabrachial nucleus	2
Raphe nuclei	2
Rostral ventral medulla	2